Article

Effect of Chromophore-Charge Distance on the Energy Transfer Properties of Water-Soluble Conjugated Oligomers

Bin Liu, Brent S. Gaylord, Shu Wang, and Guillermo C. Bazan

J. Am. Chem. Soc., **2003**, 125 (22), 6705-6714• DOI: 10.1021/ja028961w • Publication Date (Web): 10 May 2003

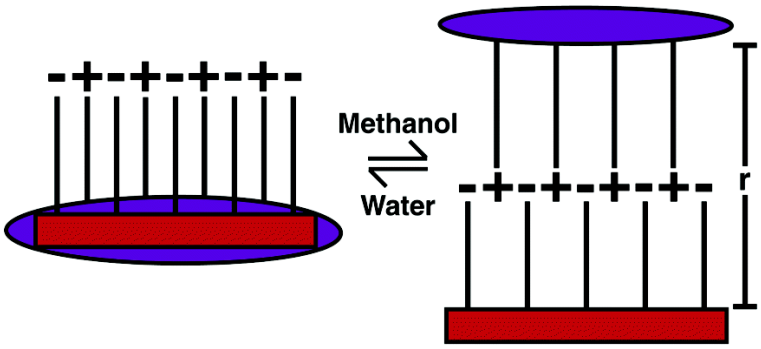

More About This Article

Additional resources and features associated with this article are available within the HTML version:

- Supporting Information
- Links to the 24 articles that cite this article, as of the time of this article download
- Access to high resolution figures
- Links to articles and content related to this article
- Copyright permission to reproduce figures and/or text from this article

View the Full Text HTML

J|A|C|S
ARTICLES
Published on Web 05/10/2003

Effect of Chromophore-Charge Distance on the Energy Transfer Properties of Water-Soluble Conjugated Oligomers

Bin Liu, Brent S. Gaylord, Shu Wang, and Guillermo C. Bazan*

Contribution from the Institute for Polymers and Organic Solids, Departments of Chemistry and Materials, University of California, Santa Barbara, California 93106

Received October 15, 2002; E-mail: bazan@chem.ucsb.edu

Abstract: The synthesis of 1,4-bis(9,9′-bis(3″-(*N*,*N*,*N*-trimethylammonium)-propyl)-2′-fluorenyl)benzene tetrabromide (**C_3**), 1,4-bis(9,9′-bis(4″-(*N*,*N*,*N*-trimethylammonium)-butyl)-2′-fluorenyl)benzene tetrabromide (**C_4**), 1,4-bis(9,9′-bis(6″-(*N*,*N*,*N*-trimethylammonium)-hexyl)-2′-fluorenyl)benzene tetrabromide (**C_6**), and 1,4-bis(9,9′-bis(8″-(*N*,*N*,*N*-trimethylammonium)-octyl)-2′-fluorenyl)benzene tetrabromide (**C_8**) is reported. Fluorescence energy transfer experiments between **C_3**−**C_8** and the acceptors pentasodium 1,4-bis(4′(2″,4″-bis(butoxysulfonate)-styryl)styryl)-2-(butoxysulfonate)-5-methoxybenzene (**3**), fluorescein labeled single-stranded DNA and fluorescein labeled double-stranded DNA in water, buffer, and methanol reveal the importance of hydrophobic and electrostatic forces in determining chromophore−chromophore close proximity. In water, the oligomers with longer side chain length show better energy transfer, as well as higher Stern−Volmer quenching constants (K_{sv}), largely due to a stronger hydrophobic attraction between the optically active components. In methanol, the differences in energy transfer are leveled, and the oligomers with shorter side chain lengths show higher K_{sv} values. Compounds **C_3**, **C_4**, **C_6**, and **C_8** were also used to dissect the different contributors to DNA hybridization assays based on cationic conjugated polymers.

Introduction

Novel techniques to determine DNA hybridization and sequence characterization are under intense investigation.[1] They find use in many applications, including medical diagnostics, examination of gene mutations, and drug delivery monitoring.[2] DNA detection methods are expected to increase in importance, as samples from patients will need to be quickly screened and compared to genomic databases. New techniques under development include homogeneous fluorescence-based DNA hybridization assays,[3] DNA microarray technology which relies on the hybridization between DNA sequences on a microarray surface,[4] the use of semiconductor crystals or quantum dots as fluorescent probes,[5−7] nanoparticle-amplified surface plasmon resonance (SPR) techniques,[8−10] and the use of redox-active nucleic acid replica for amplified bioelectrocatalytic DNA detection.[11]

Fluorescence-based detection methods are well established but continue to be optimized for enhanced sensitivity and for simplified protocols.[12] Homogeneous methods, in particular, require less manipulation after exposure to the target DNA and avoid difficulties associated with attaching the probe to a surface.[13] Assays based on Förster energy transfer, also known as fluorescence resonance energy transfer (FRET), in which the distance between a donor and an acceptor changes when the target strand is present, have been used for some time.[12] Traditional energy/electron transfer pairs for strand specific assays require dual modification of the same DNA strand, which can result in singly labeled impurities, lower yields, and more difficult probe purification protocols.[14,15] These considerations make the development of simple and economic methods that utilize the ease of homogeneous fluorescence assays with minimal DNA modification highly desirable.

Work in the field of gene delivery has elucidated the strong interaction between cationic polyelectrolytes and negatively charged DNA strands.[16] The spontaneous formation of these interpolymer complexes is thought to be primarily the result of cooperative electrostatic forces; however, the importance of

(1) (a) Dubertret, B.; Calame, M.; Libchaber, A. *Nat. Biotechnol.* **2001**, *19*, 365. (b) Wang, J. *Nucleic Acids Res.* **2000**, *28*, 3011. (c) Cardullo, R. A.; Agrawal, S.; Flores, C.; Zamecnik, P. C.; Wolf, D. E. *Proc. Natl. Acad. Sci. U.S.A.* **1988**, *85*, 8790. (d) Umek, R. M.; Lin, S. W.; Vielmetter, J.; Terbrueggen, R. H.; Irvine, B.; Yu, C. J.; Kayyem, J. F.; Yowanto, H.; Blackburn, G. F.; Farkas, D. H.; Chen, Y. P. *J. Mol. Diagn.* **2001**, *3*, 74. (e) Schork, N. J.; Fallin, D.; Lanchbury, J. S. *Clin. Genet.* **2000**, *58*, 250.
(2) Balakin, K. V.; Horshun, V. A.; Mikhalev, I. I.; Maleev, G. V.; Malakhov, A. D.; Prokhorenko, J. A.; Berlin, Yu. A. *Biosens. Bioelectron.* **1998**, *13*, 771.
(3) Sueda, S.; Yuan, J.; Matsumoto, K. *Bioconjugate Chem.* **2002**, *13*, 200 and references therein.
(4) Niemeyer, C. M.; Blohm, D. *Angew. Chem., Int. Ed.* **1999**, *38*, 2865.
(5) Gerion, D.; Parak, W. J.; Williams, S. C.; Zanchet, D.; Micheel, C. M.; Alivisatos, A. P. *J. Am. Chem. Soc.* **2002**, *124*, 7070.
(6) Bruchez, M.; Moronne, M.; Gin, P.; Weiss, S.; Alivisatos, A. P. *Science* **1998**, *281*, 2013.
(7) Chan, W. C. W.; Nie, S. M. *Science* **1998**, *281*, 2016.
(8) He, L.; Musick, M. D.; Nicewarner, S. R.; Salinas, F. G.; Benkovic, S. J.; Natan, M. J.; Keating, C. D. *J. Am. Chem. Soc.* **2000**, *122*, 9071.
(9) Nelson, B. P.; Grimsrud, T. E.; Liles, M. R.; Goodman, R. M.; Corn, R. M. *Anal. Chem.* **2001**, *73*, 1.
(10) Tombelli, S.; Minunni, M.; Mascini, M. *Anal. Lett.* **2002**, *35*, 599.
(11) (a) Patolsky, F.; Weizmann, Y.; Willner, I. *J. Am. Chem. Soc.* **2002**, *124*, 770. (b) Caruana, D. J.; Hellerr, A. *J. Am. Chem. Soc.* **1999**, *121*, 769.
(12) Lakowicz, J. R. *Principles of Fluorescence Spectroscopy*, 2nd ed.; Kluwer Academic/Plenum Publisher: New York, 1999.
(13) Paris, P. L.; Langenhan, J. M.; Kool, E. T. *Nucleic Acids Res.* **1998**, *26*, 3789.
(14) Knemeyer, J.; Marm, N.; Sauer, M. *Anal. Chem.* **2000**, *72*, 3717.
(15) Castro, A.; Williams, J. G. K. *Anal. Chem.* **1997**, *69*, 3915.
(16) Kabanov, A. V., Felgner, P., Seymour, L. W., Eds. *Self-Assembling Complexes for Gene Delivery. From Laborotary to Clinical Trial*; John Wiley: Chichester, 1998.

Scheme 1. Molecular Structures of **1**−**3**

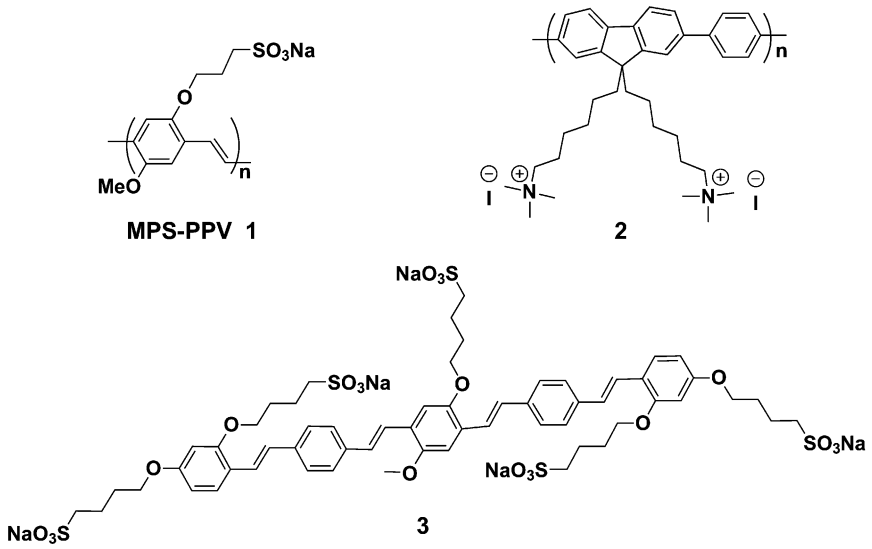

hydrophobic interactions between aromatic polymer units and DNA bases has also been recognized.[17] The overall free energy of these interactions is controlled by the molecular structure of the participating species, in conjunction with variables such as pH, ionic strength, and temperature.[18−20] Despite the complexity of these interactions, synthetic polycations have recently been shown to recognize the tertiary structure of plasmid DNA.[18] Cationic polyelectrolytes have also been studied because of their effect on the fluorescence of oppositely charged acceptor complexes.[21,22] After complexation with DNA, positively charged synthetic polyelectrolytes change the fluorescence emission and energy transfer processes when the polyelectrolyte is tagged with a chromophore such as pyrene.[2]

Conjugated polymers provide highly responsive optical platforms for chemical and biological detection.[23,24] Water-soluble conjugated polymers[25] are of particular interest for reporting biological recognition events. Polymers such as the anionic MPS-PPV (**1**, in Scheme 1) and the cationic poly(9,9-bis(6′-*N*,*N*,*N*-trimethylammonium)hexyl)-fluorene phenylene) (**2**) have shown extremely large quenching efficiencies in the presence of oppositely charged acceptors.[23,26,27]

Cationic polymers such as **2** form part of a DNA-sensor technique which utilizes the optical amplification of conjugated polymers and the complexation of oppositely charged polyelectrolytes (Scheme 2).[28,29] In this method, one excites the conjugated polymer and compares the emission of a dye (C*)

Scheme 2. DNA Hybridization Assay Based on FRET from a Water-Soluble Cationic Conjugated Polymer to a Fluorophore-Tagged ssDNA Probe

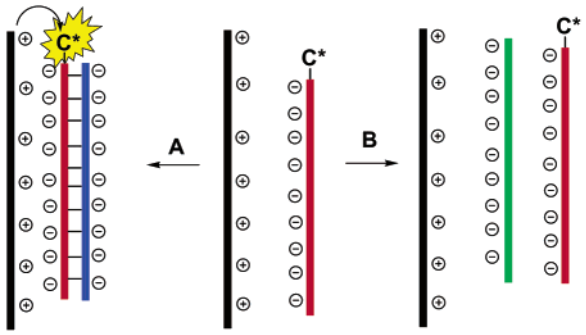

attached to the probe single-stranded DNA (shown in red) to that of the conjugated polymer (shown in black). The optical properties of the components are chosen so that only the polymer absorbs at the excitation frequency and the absorption of C* overlaps the emission from the polymer (FRET condition). Hybridization of the probe strand to its complementary strand (shown in blue) results in a more efficient FRET *ratio* than when a noncomplementary strand (shown in green) is added to the solution. Furthermore, that the emission of the dye is stronger when exciting the conjugated polymer than upon direct dye excitation demonstrates the light-harvesting properties of the conjugated polymer.[24,30,31]

In this contribution, we probe how the distance between the positively charged trimethylalkylammonium group and the conjugated chromophore influences the FRET to fluorophore-tagged DNA. To eliminate inherent problems associated with controlling polymer chain length and molecular weight distributions, we focus on well-defined conjugated oligomers with the bis(fluorenyl)benzene structure. The general structure of these molecules is shown below.

We will examine the energy transfer process to a pentaanionic chromophore (**3** in Scheme 1), to establish the role of hydro-

(17) Ganachaud, F.; Elaïssari, A.; Pichot, C.; Laayoun, A.; Cros, P. *Langmuir* **1997**, *13*, 701.
(18) Bronich, T. K.; Nguyen, H. K.; Eisenberg, A.; Kabanov, A. V. *J. Am. Chem. Soc.* **2000**, *122*, 8339.
(19) Kuhn, P. S.; Barbosa, M. C.; Yan, L. *Physica A* **2000**, *283*, 113.
(20) Wolfert, M. A.; Dash, P. R.; Nazarova, O.; Oupicky, D.; Seymour, L. W.; Smart, S.; Strohalm, J.; Ulbrich, K. *Bioconjugate Chem.* **1999**, *10*, 993.
(21) Song, X. D.; Wang, H. L.; Shi, J.; Park, J. W.; Swanson, B. I. *Chem. Mater.* **2002**, *14*, 2342.
(22) Wang, D. L.; Gong, X.; Heeger, P. S.; Rininsland, F.; Bazan, G. C.; Heeger, A. J. *Proc. Natl. Acad. Sci. U.S.A.* **2002**, *99*, 49.
(23) Chen, L.; Mcbranch, D. W.; Wang, H. L.; Helgeson, R.; Wudl, F.; Whitten, D. G. *Proc. Natl. Acad. Sci. U.S.A.* **1999**, *96*, 12287.
(24) McQuade, D. T.; Pullen, A. E.; Swager, T. M. *Chem. Rev.* **2000**, *100*, 2537.
(25) Pinto, M. R.; Schanze, K. S. *Synthesis-Stuttgart* **2002**, *9*, 1293.
(26) Wang, J.; Wang, D.; Miller, E. K.; Moses, D.; Bazan, G. C.; Heeger, A. J. *Macromolecules* **2000**, *33*, 5153.
(27) Stork, M. S.; Gaylord, B. S.; Heeger, A. J.; Bazan, G. C. *Adv. Mater.* **2002**, *14*, 361.
(28) Gaylord, B. S.; Heeger, A. J.; Bazan, G. C. *J. Am. Chem. Soc.* **2003**, *125*, 896.
(29) For an alternate use of conjugated polymers in DNA detection, see: Ho, H. A.; Boissinot, M.; Bergeron, M. G.; Corbeil, G.; Dore, K.; Boudreau, D.; Leclerc, M. *Angew. Chem., Int. Ed.* **2002**, *41*, 1548.
(30) McQuade, D. T.; Hegedus, A. H.; Swager, T. M. *J. Am. Chem. Soc.* **2000**, *122*, 12389.
(31) Yang, J. S.; Swager, T. M. *J. Am. Chem. Soc.* **1998**, *120*, 11864.

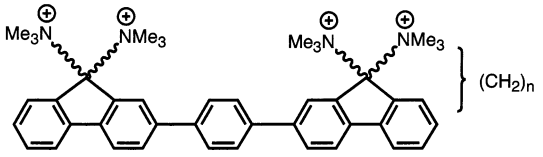

C_3, n = 3; C_4, n = 4; C_6, n = 6; C_8, n = 8

phobic forces and electrostatic interactions. We next probe how chromophore-tagged single-stranded DNA (ssDNA) and double-stranded DNA (dsDNA) behave as FRET acceptors. Finally, we compare situations where complementary and noncomplementary strands are added to the ssDNA carrying the acceptor chromophore to dissect the different forces operating in biosensor protocols such as those shown in Scheme 2.

Results and Discussion

Synthesis and Characterization. The synthetic approach to oligomers, 1,4-bis(9,9′-bis(3″-(*N*,*N*,*N*-trimethylammonium)-propyl)-2′-fluorenyl)benzene tetrabromide (**C_3**), 1,4-bis(9,9′-bis(4″-(*N*,*N*,*N*-trimethylammonium)-butyl)-2′-fluorenyl)benzene tetrabromide (**C_4**), 1,4-bis(9,9′-bis(6″-(*N*,*N*,*N*-trimethylammonium)-hexyl)-2′-fluorenyl)benzene tetrabromide (**C_6**), and 1,4-bis(9,9′-bis(8″-(*N*,*N*,*N*-trimethylammonium)-octyl)-2′-fluorenyl)benzene tetrabromide (**C_8**), is shown in Scheme 3. Treatment of 2-bromofluorene with 50% KOH, followed by reaction with excess α,ω-dibromoalkane, provides compounds 2-bromo-9,9′-bis(3″-bromopropyl)fluorene (**4**), 2-bromo-9,9′-bis(6″-bromohexyl)fluorene (**5**), and 2-bromo-9,9′-bis(8″-bromooctyl)fluorene (**6**) in yields of 35−80%. Instead of forming the desired 2-bromo-9,9′-bis(4′-bromobutyl)fluorene, the direct treatment of 2-bromofluorene with KOH and 1,4-dibromobutane produces 2-bromo-9,9-*gem*-cyclopentyl cleanly. To circumvent this complication, 1,4-dibromobutane was first treated with 1 equiv of 4-methylphenol to give 4-bromo-1-(4′-methylphenoxy)butane (**7**) in approximately 80% yield.[32] An excess of **7** was subsequently reacted with deprotonated 2-bromofluorene to form intermediate **8**, which can be subsequently transformed into 2-bromo-9,9′-bis(4″-bromobutyl)fluorene (**9**) by treatment with hydrobromic acid in acetic acid under refluxing conditions over a period of 2 days.[32]

Coupling of 2 equiv of **4**, **5**, **6**, or **9** with 1,4-phenyldiboronic acid under Suzuki coupling conditions using $Pd(PPh_3)_4$ in refluxing THF/H_2O (2:1) over 36 h gives oligomers 1,4-bis-(9,9′-bis(3″-bromopropyl)-2′-fluorenyl)benzene (**10**), 1,4-bis-(9,9′-bis(4″-bromobutyl)-2′-fluorenyl)benzene (**11**), 1,4-bis(9,9′-bis(6″-bromohexyl)-2′-fluorenyl)benzene (**12**), and 1,4-bis(9,9′-bis(8″-bromooctyl)-2′-fluorenyl)benzene (**13**) in 45−60% yields. Formation of **C_3**, **C_4**, **C_6**, and **C_8** from **10**, **11**, **12**, and **13**, respectively, was achieved by using condensed trimethylamine in THF/H_2O (2:1) mixture. As compared to our previous report, which involved addition of a methylhalide, such as MeI, to 1,4-bis(9,9′-bis(6″-(*N*,*N*-dimethylamino)hexyl)-2′-fluorenyl)benzene, the new procedure bypasses the need to prepare trialkylamino-substituted oligomers.[27] The alkylamino intermediates are highly polar and adsorb strongly to chromatographic supports, which makes their purification considerably more complicated and reduces reaction yields.

The ^{1}H NMR spectroscopy signals of **C_3**−**C_8** at room temperature are broad and indistinguishable, presumably due to aggregation at concentrations useful for good signal-to-noise ratios (10^{-2}−10^{-4} M). Therefore, the spectra for the oligomers **C_3**−**C_8** were measured at elevated temperatures in D_2O. Integration of the ^{1}H NMR signals of **C_3** at 90 °C indicates >99% quaternization, by comparison against the integrated values for −CH_2N and −NCH_3 peaks at 3.52 and 3.30 ppm, respectively. In the case of **C_4**, **C_6**, and **C_8**, because the signals for the methylene-N and the methylamino protons overlap, the degree of quaternization was calculated by the ratio of −CH_2N and −NCH_3 (∼3.40 ppm) to the characteristic methylene groups (∼1.90 ppm) at the 9-position of fluorene. Further evidence of the identity of **C_3**−**C_8** was obtained by electrospray ionization mass spectrometry (ESI-MS). Peaks corresponding to the correct molecular structures were detected for the four oligomers.

Table 1 shows the absorption and emission data for oligomers **3** and **C_3**−**C_8**. For the neutral precursors **10**−**13**, there is no difference in the absorption maxima in chloroform (λ_{max} = 330 nm). In water, the absorption maxima range from 329 nm for **C_3** to 336 nm for **C_8**. The blue shift with decreasing distance to the positive charge is likely due to a combination of electronic effects and perhaps a decreased level of aggregation for oligomer **C_3**. Tether length, however, does not influence the fluorescence properties of the chromophores; the emission of **C_3**−**C_8** in water occurs at ∼396 nm, with a calculated quantum efficiency of 65 ± 5%.

Table 1 also contains the data for absorption and emission maxima of the oligomers in methanol. The emission occurs at the same frequency for the four oligomers. We note that the fluorescence efficiency of oligomers **C_3**−**C_8** in methanol (70 ± 5% using 9,10-diphenylanthracene in cyclohexane as the standard) is slightly higher than that measured in water (Table 1), consistent with less aggregation in methanol, relative to water.

The synthesis of pentasodium 1,4-bis(4′(2″,4″-bis(butoxysulfonate)-styryl)styryl)-2-(butoxysulfonate)-5-methoxybenzene (**3** in Scheme 1) has been reported previously.[33]

Förster Energy Transfer between C_3−C_8 and 3. The absorption spectrum of **3** in water overlaps the emission spectra of oligomers **C_3**−**C_8** (Table 1); thus efficient Förster energy transfer should be expected between these molecules.[12,27] Indeed, when **3** is added to the oligomer solutions, one observes a decrease in the emission of **C_3**−**C_8**, with a concomitant increase in the emission of **3**. Figure 1 shows the fluorescence changes upon addition of **3** to **C_8** ([**C_8**] = 2.0×10^{-6} M), [**3**] varies from 3.0×10^{-8} to 1.0×10^{-6} M). Similar changes in emission spectra were obtained with solutions of **C_3**−**C_6**. In these mixtures, **3** acts as the acceptor, and the 1,4-bis(fluorenyl)-benzene chromophore acts as the donor.

Stern−Volmer analysis gives insight into the efficiency of fluorescence quenching or energy transfer according to the equation:

$$PL_0/PL = 1 + K_{sv}[Q]$$

where PL_0 and PL correspond to the integrated emission of the bis(fluorenyl)benzene chromophore in the absence and presence of **3**, respectively.[12] A plot of PL_0/PL versus [**3**] in water, with [**C_3**−**C_8**] = 2.0×10^{-6} M, is shown in Figure 2.

(32) Rau, I. U.; Rehahn, M. *Acta Polym.* **1994**, *45*, 3.

(33) Gaylord, B. S.; Wang, S.; Heeger, A. J.; Bazan, G. C. *J. Am. Chem. Soc.* **2001**, *123*, 6417.

Scheme 3. General Synthetic Scheme for the Preparation of Compounds $\mathbf{C_3}-\mathbf{C_8}$[a]

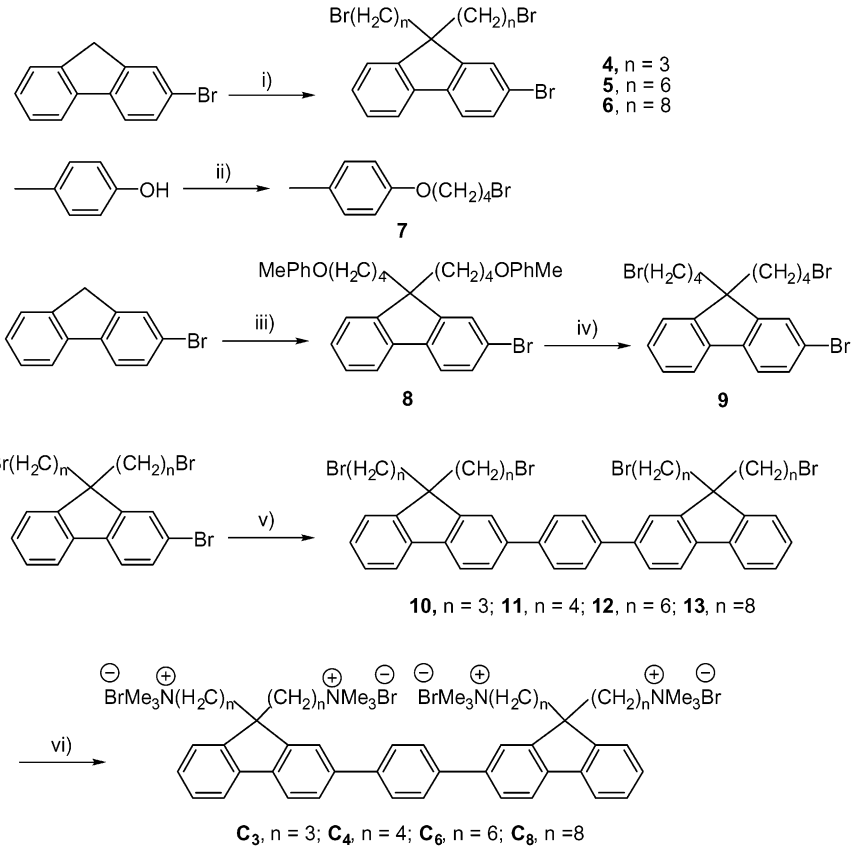

[a] (i) $KOH/H_2O/Br(CH_2)_nBr$; (ii) K_2CO_3/18-crown-6/$Br(CH_2)_4Br$; (iii) KOH/H_2O/**7**; (iv) HBr/CH_3COOH; (v) 1,4-$(B(OH)_2)_2$-$C_6H_4/Pd(PPh_3)_4/Na_2CO_3$/$THF/H_2O$; (vi) $NMe_3/THF/H_2O$.

Table 1. Absorption and Fluorescence Data

	λ_{max} (nm)[a]		λ_{max} (nm)[b]		QE[c] (±5%)		K_{sv} (M^{-1})	
compound	water	methanol	water	methanol	water	methanol	water	methanol
3	410	413	504	477, 507	10%	56%		
$\mathbf{C_3}$	329	332	394	373, 393	64%	76%	9.02×10^5	1.81×10^6
$\mathbf{C_4}$	330	332	395	373, 393	66%	75%	9.26×10^5	1.75×10^6
$\mathbf{C_6}$	334	332	396	373, 393	66%	75%	1.52×10^6	1.54×10^6
$\mathbf{C_8}$	336	332	396	373, 393	65%	74%	2.07×10^6	1.46×10^6

[a] Absorption. [b] Emission. [c] Using 9,10-diphenylanthracene as the standard.

In the Stern−Volmer plots, the fluorescence intensity was corrected for any changes in absorbance. A linear region is observed at low quencher concentrations, followed by an upsloping nonlinear region where the energy transfer may be described by a "sphere of action" mechanism.[26] From the slope of the linear region ([**3**] = 0 to 3×10^{-7} M) of the plots, one obtains the Stern−Volmer constant K_{sv}, which provides a measure of the rate for quenching or energy transfer. In water, oligomer $\mathbf{C_8}$ exhibits the highest K_{sv} (2.07×10^6 M^{-1}, Table 1). The next highest value corresponds to $\mathbf{C_6}$ (1.52×10^6 M^{-1}), while the difference between $\mathbf{C_3}$ and $\mathbf{C_4}$ falls within experimental uncertainty (9.02×10^5 and 9.26×10^5 M^{-1}). At the same concentration of **3**, $\mathbf{C_8}$ gives the highest emission intensity from the acceptor. These differences are illustrated in Figure 3, which shows the emission spectra from solutions containing [**3**] = 7.9×10^{-7} M and [$\mathbf{C_3}-\mathbf{C_8}$] = 2.0×10^{-6} M. These studies show that in water the molecules with the *longest tether* give rise to the *most efficient* energy transfer process.

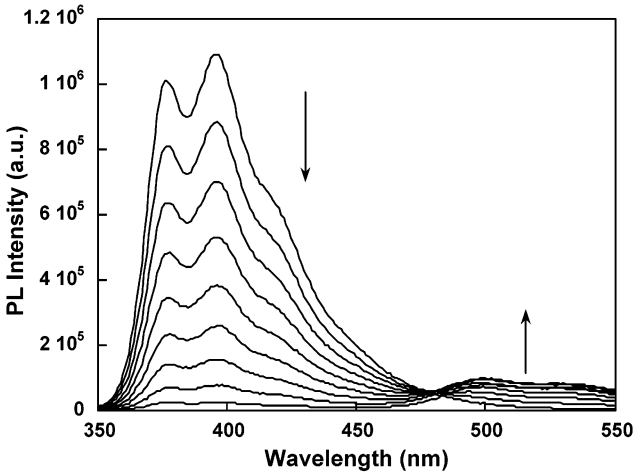

Figure 1. Emission spectra for mixtures of $\mathbf{C_8}$ with **3** in water. [$\mathbf{C_8}$] = 2.0×10^{-6} M, [**3**] = 3.0×10^{-8} M to 1.0×10^{-6} M.

As reported earlier for **3** and 1,4-bis(9,9′-bis(6″-(*N*,*N*,*N*-trimethylammonium)hexyl)-2′-fluorenyl)benzene tetraiodide, that is, oligomer $\mathbf{C_6}$ with iodide counteranions, the fluorescence quenching mechanism is dominated by the formation of a ground-state complex.[27] This interaction is favored by the ion pairing between the positively charged donor and the negative acceptor. Oligomer **3**, however, aggregates in water, giving rise to large (∼190 nm) clusters, even at concentrations as low as 10^{-5} M.[33] The formation of these aggregates is driven by the hydrophobic nature of the conjugated chromophore framework. It is reasonable to expect a similar contribution from hydro-

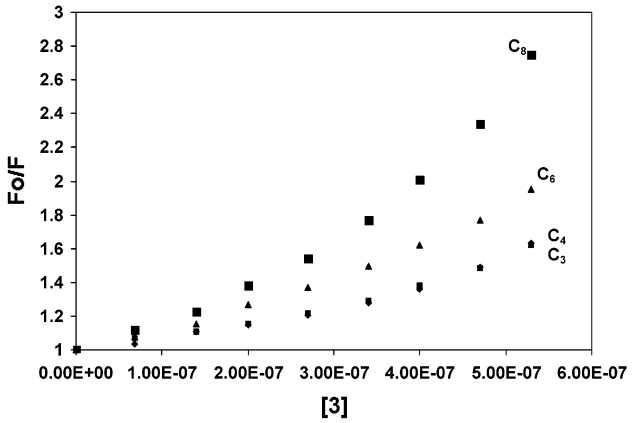

Figure 2. Stern−Volmer plot in water for $[\mathbf{C_3}-\mathbf{C_8}] = 2.0 \times 10^{-6}$ M with $[\mathbf{3}] = 0$ to 5.0×10^{-6} M. The emission spectra were measured by exciting at the absorption maximum of $\mathbf{C_3}-\mathbf{C_8}$.

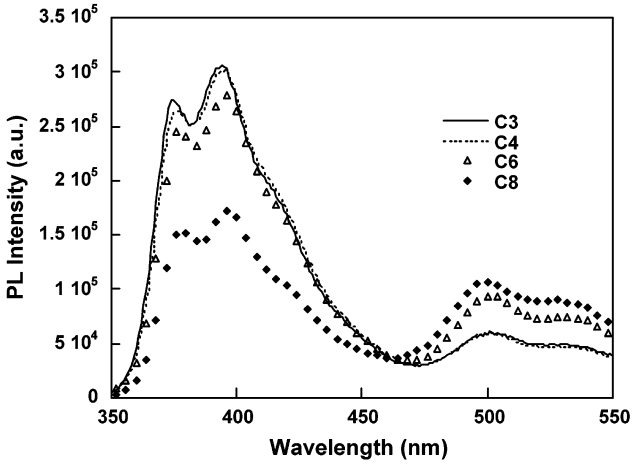

Figure 3. FRET comparison from $\mathbf{C_3}-\mathbf{C_8}$ to **3** in water. $[\mathbf{C_3}-\mathbf{C_8}] = 2.0 \times 10^{-6}$ M and $[\mathbf{3}] = 7.9 \times 10^{-7}$ M. The emission spectra were measured by exciting at the absorption maximum of $\mathbf{C_3}-\mathbf{C_8}$.

phobic forces in the fluorescence quenching of $\mathbf{C_3}-\mathbf{C_8}$ by **3**. Furthermore, the larger molecular volume is expected to provide diminished charge density in the case of $\mathbf{C_8}$.[34] The enhanced energy transfer observed for $\mathbf{C_8}$ strongly suggests that the larger hydrophobic component in $\mathbf{C_8}$ is responsible for closer contacts with **3**, when compared to $\mathbf{C_3}$.

To further examine the importance of hydrophobic forces and the role of the medium, we evaluated the K_{sv} constants in methanol. This solvent is sufficiently polar to dissolve the charged chromophores, but, because of its organic nature, it should decrease the aggregation of the organic fragments. Table 1 shows that the K_{sv} values are of the same magnitude as those obtained in water. However, the order of K_{sv} values is reversed; $\mathbf{C_3}$ is quenched more readily, whereas $\mathbf{C_8}$ shows the smallest K_{sv}.

That the sequence of K_{sv} magnitude for the oligomers follows opposite structural trends in water and methanol highlights the interplay between hydrophobic and electrostatic forces. It is reasonable that, with increased side chain length, the oligomer becomes more hydrophobic. The differences in K_{sv} between methanol and water as a function of tether length can be rationalized in terms of several phenomena such as aggregation

(34) Israelachvili, J. *Intermolecular & Surface Forces*, 2nd ed.; Harcourt Brace & Company, Publisher: Orlando, FL, 1992.

Scheme 4. Schematic Diagram Which Shows the Preferred Average Intermolecular Associations in Water and in Methanol

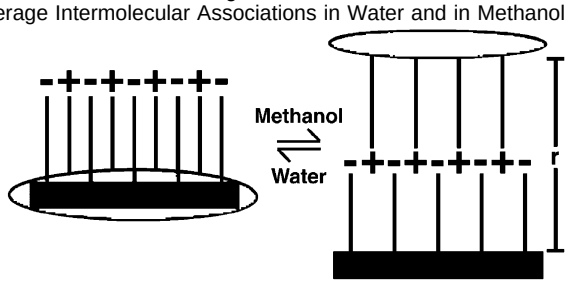

size, electronic communication between subunits in the aggregate, and the proximity between donor and acceptor. However, we propose a simple picture that accounts for the trends by focusing on the two extreme cases of $\mathbf{C_3}$ and $\mathbf{C_8}$. The larger hydrophobic content of $\mathbf{C_8}$, relative to $\mathbf{C_3}$, increases the aggregate size in water and also the hydrophobic interactions between the optically active parts of **3** and $\mathbf{C_8}$. We show the relationship in Scheme 4, with the charges pairing up and the organic portions coming together in aqueous media. In methanol, the hydrophobic contacts between the organic units are considerably reduced, and the electrostatic interactions dominate the order of rank of K_{sv} magnitudes. The more efficient energy transfer from $\mathbf{C_3}$ results from its shorter tether length, which brings the two chromophores closer together, and the $1/r^6$ dependence of Förster energy transfer.[12]

Comparison of Figure 4 to Figure 1 shows more emission from **3** in methanol, relative to that in water. These observations are consistent with the higher quantum efficiency of **3** in methanol (56 ± 5%), relative to that in water (10 ± 5%).

Energy Transfer Studies between Oligomers and ssDNA-C*. As discussed in the Introduction, our interest in probing the basic energy transfer characteristics of $\mathbf{C_3}-\mathbf{C_8}$ stems from the use of cationic conjugated polymers in DNA hybridization assays.[28] We now examine the effect of the tether length on fluorescence quenching with a ssDNA labeled with an acceptor chromophore.[35] The oligonucleotide used is 5′-Fl-CCA ATC AGT CCA GTG ATA CG (ssDNA-C*), with fluorescein (C*) at the 5′ position. The spectra in Figure 5 show the overlap between the emission of $\mathbf{C_3}-\mathbf{C_8}$ and the absorption of ssDNA-C* in the 350−530 nm range. While this spectral overlap is not as extensive as that between $\mathbf{C_3}-\mathbf{C_8}$ and **3**, it is sufficient to examine the dependence of FRET on the molecular structure and solvent medium.

Only the $\mathbf{C_6}$/ssDNA-C* and $\mathbf{C_8}$/ssDNA-C* combinations show sufficient C* emission to be detected using a standard fluorometer (Figure 6). Measurements were carried out in buffer (0.1 M sodium chloride + 0.01 M sodium citrate) and at a fixed ssDNA-C* concentration (2.0×10^{-8} M), with the donor concentration varying from 2.0×10^{-8} to 2.0×10^{-7} M. The emission maxima of the C* in the $\mathbf{C_6}$/ssDNA-C* and $\mathbf{C_8}$/ssDNA-C* mixtures are red-shifted ($\lambda = 527$ nm) relative to its emission when excited directly in the absence of the donor oligomers ($\lambda = 517$ nm). This emission red shift indicates

(35) Fluorescein was chosen because it is one of the most ubiquitous dyes used in FRET experiment and because it can be easily attached to DNA. Its fluorescence and absorbance properties are known to be pH dependent, and the highest quantum yield is obtained for the fluorescein dianion. The pH of the buffer (0.1 M sodium chloride + 0.01 M sodium citrate) used for this study is about 8.3. In our experiment, the quantum yield of ssDNA-C* was determined to be 94%, using 9,10-diphenylanthracene as the standard.

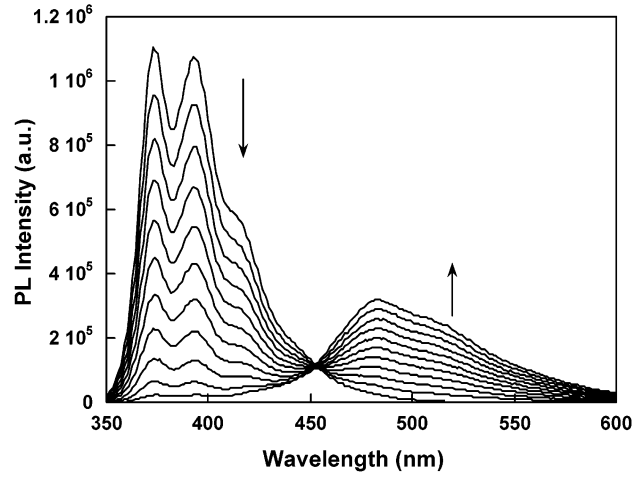

Figure 4. Emission spectra for mixtures of $\mathbf{C_8}$ with **3** in methanol, $[\mathbf{C_8}] = 2.0 \times 10^{-6}$ M, $[\mathbf{3}] = 3.0 \times 10^{-8}$ to 1.2×10^{-6} M.

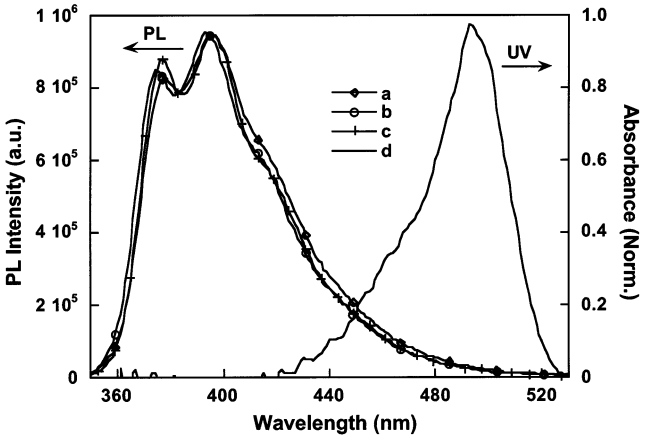

Figure 5. Spectral overlap between the photoluminescence of $\mathbf{C_3}$ (a), $\mathbf{C_6}$ (b), and $\mathbf{C_8}$ (c) and the absorbance of ssDNA-C* (d).

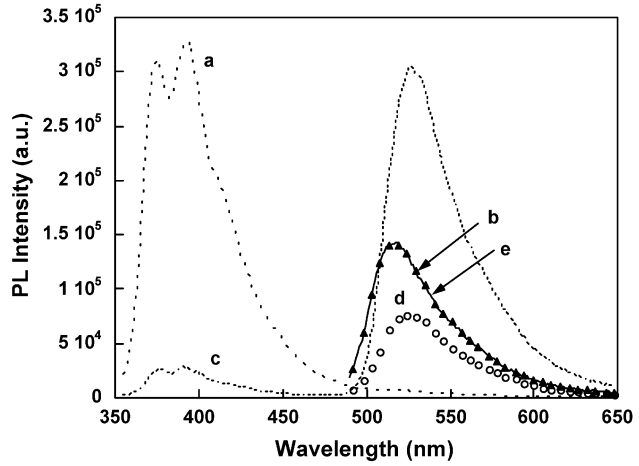

Figure 6. Emission for the $\mathbf{C_3}$/ssDNA-C* (a and b) or $\mathbf{C_8}$/ssDNA-C* (c and d) solutions obtained by exciting at two different wavelengths, 345 nm (a and c) and 480 nm (b and d). The conditions for this comparison are $[\text{ssDNA-C*}] = 2.0 \times 10^{-8}$ M, $[\mathbf{C_3}] = [\mathbf{C_8}] = 8.0 \times 10^{-8}$ M. The emission for ssDNA-C* (e) is also shown for comparison (excited at 480 nm). Note that the spectra in (b) and (e) overlap each other exactly.

complex formation and the close proximity of the cationic structure, which changes the polarity near fluorescein. Direct excitation at 480 nm in the presence of $\mathbf{C_3}$ or $\mathbf{C_4}$ results in emission at 517 nm. Thus, in buffer, the $\mathbf{C_3}$/ssDNA-C* and $\mathbf{C_4}$/ssDNA-C* combinations do not lead to complex formation.

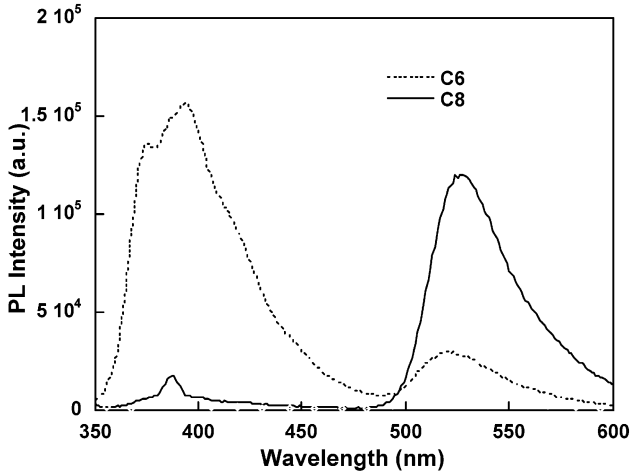

Figure 7. FRET comparison for solutions containing ssDNA-C* and $\mathbf{C_6}$ or $\mathbf{C_8}$ in buffer ($[\text{ssDNA-C*}] = 2.0 \times 10^{-8}$ M, $[\mathbf{C_6}] = [\mathbf{C_8}] = 8.0 \times 10^{-8}$ M). The fluorescence spectra were measured by exciting at 345 nm.

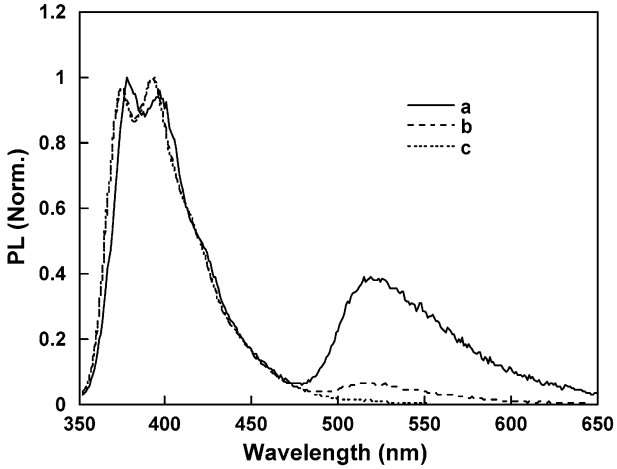

Figure 8. Effect of ionic strength on the FRET between $\mathbf{C_3}$ and ssDNA-C*. The emission of $\mathbf{C_3}$ is normalized for comparison. The concentration of NaCl ranges from 0 to 0.1 M, with $a = 0$ M, $b = 0.02$ M, and $c = 0.1$ M.

Figure 7 shows a direct comparison of the emission in buffer upon excitation of $\mathbf{C_6}$ or $\mathbf{C_8}$ in the presence of ssDNA-C*. The C* emission is 6 times more intense for $\mathbf{C_8}$/ssDNA-C* than for $\mathbf{C_6}$/ssDNA-C*. Under similar $[\mathbf{C_8}]$ or $[\mathbf{C_6}]$, there is no fluorescein emission when free fluorescein is used. This demonstrates that the ssDNA structure plays an important role in bringing the donor and C* together.

Energy transfer is observed from the four oligomers to the ssDNA-C* in *pure water*. The absence of buffer ions under these conditions allows electrostatic forces to bring the two opposite charged molecules into close proximity.[26] Addition of NaCl to $\mathbf{C_3}$/ssDNA-C* solutions results in a decrease of C* emission and an increase of $\mathbf{C_3}$ emission (Figure 8). Note that the data in Figure 8 are normalized relative to oligomer emission to highlight the decrease in C* emission. At 0.1 M NaCl, C* emission is absent, indicating ionic screening of the $\mathbf{C_3}$/DNA-C* attraction. The C* emission under these conditions, obtained by direct excitation, occurs at 517 nm, giving further evidence of the absence of complexation. For the $\mathbf{C_8}$/ssDNA-C* mixture, when the NaCl concentration reaches 0.2 M, only 30% of the emission from fluorescein is lost, and it is still detectable even when the NaCl concentration reaches 1.07 M (Figure 9).

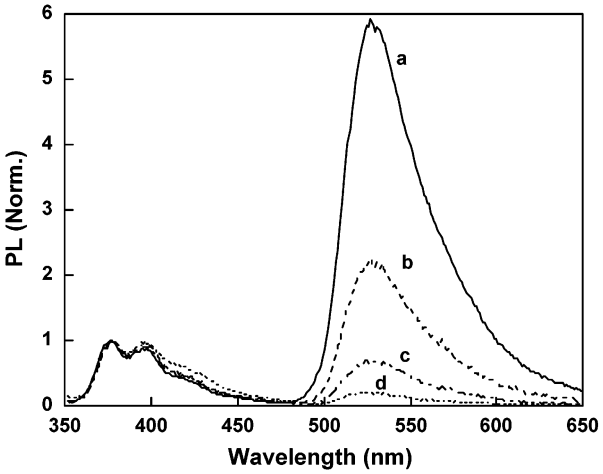

Figure 9. Effect of ionic strength on the FRET between $\mathbf{C_8}$ and ssDNA-C*. The emission of $\mathbf{C_8}$ is normalized for comparison. The concentration of NaCl ranges from 0 to 1.07 M, with $a = 0$ M, $b = 0.20$ M, $c = 0.46$ M, and $d = 1.07$ M.

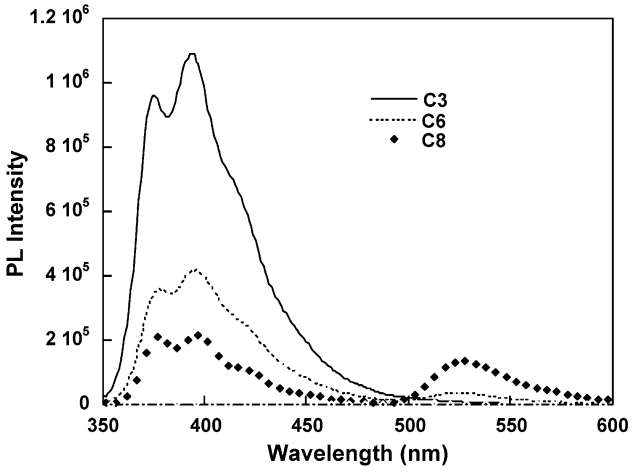

Figure 10. FRET comparison for solutions containing $dsDNA_2$-C* and $\mathbf{C_3}$, $\mathbf{C_6}$, or $\mathbf{C_8}$ in buffer. [$dsDNA_2$-C*] $= 2.0 \times 10^{-8}$ M, [$\mathbf{C_n}$] $= 1.6 \times 10^{-7}$ M. The excitation wavelength was 345 nm for all spectra.

In pure water or in buffer (0.1 M NaCl + 0.01 M sodium citrate), the maximum emission intensity from C* obtained by energy transfer from $\mathbf{C_8}$ was achieved when the ratio of cationic to anionic charges was slightly larger than 1 (1.1−1.4). In these experiments, the ssDNA-C* concentration was kept constant, and $\mathbf{C_8}$ was added incrementally. Once the charge ratio increases beyond ~1.2, the $\mathbf{C_8}$ emission increases sharply, and only a small enhancement occurs for the C* emisson. Indeed, the emission of $\mathbf{C_8}$ in buffer was essentially quenched until the charge ratio reaches 1.2. Such a charge ratio dependence on dye emission intensity should be expected because when [$\mathbf{C_8}$]/[ssDNA-C*] < 1, not all of the ssDNA-C* strands can be in close proximity to the donor oligomer units. Conversely, in the [$\mathbf{C_8}$]/[ssDNA-C*] > 1 regime, not all of the photons harnessed by **1** (the donor) can be transferred to the ssDNA-C* acceptor. A similar dependence of charge ratio on C* intensity was observed when examining the efficiency of energy transfer from the cationic conjugated polymer **2** and DNA-C* or PNA-C* (PNA = peptide nucleic acid, C* = fluorescein) hybridized with DNA.[28,36]

Energy Transfer between $\mathbf{C_8}$ and Double-Stranded DNA (dsDNA). When ssDNA-C* is hybridized with a complementary strand, the resulting double-stranded DNA (dsDNA) has a more rigid and more compact structure and exhibits an increased charge density.[37] In double-stranded DNA, the hydrophobic bases are packed inside the helix, which minimizes external hydrophobic interactions. The exposed bases in single-stranded DNA, however, more readily enable hydrophobic interactions.[38] Initial hybridization of the ssDNA-C* oligonucleotide probe described in the previous section (5′-Fl-CCA ATC AGT CCA GTG ATA CG) with the complementary strand leads to a dsDNA-C*, in which the C* emission, upon direct excitation at 480 nm, is 55% of the emission observed from ssDNA-C*. This efficiency loss is due to the quenching by the guanine in the complementary strand, which is spatially adjacent to C* after hybridization.[39,40] To examine the role of dsDNA, we designed a new single-stranded DNA probe sequence, 5′-Fl-ATC TTG ACT ATG TGG GTG CT, which would not quench the emission of the fluorescein upon hybridization. Indeed, the direct excitation of the new double-stranded DNA ($dsDNA_2$-C*) shows a fluorescence efficiency for fluorescein which is only 10% lower than the $ssDNA_2$-C*. We therefore focused our energy transfer studies on $dsDNA_2$-C*.

Figure 10 shows that, in buffer, the ability to energy transfer to $dsDNA_2$-C* follows the order $\mathbf{C_8} > \mathbf{C_6}$, with no FRET observed with $\mathbf{C_3}$ (or $\mathbf{C_4}$, not shown). This dependence on molecular structure is similar to that observed with the ssDNA experiments. Upon excitation at 345 nm, the emission maximum of $\mathbf{C_8}$/$dsDNA_2$-C* is 18 nm red-shifted relative to the direct excitation of the $dsDNA_2$-C* in the absence of the donor. At concentrations of [$dsDNA_2$-C*] $= 2.0 \times 10^{-8}$ M and [$\mathbf{C_8}$] $= 3.0 \times 10^{-7}$ M, the integrated C* emission is 3-fold greater than that obtained by directly exciting the chromophore at its maximum absorption in the absence of the donor.

We now dissect the DNA biosensor process shown in Scheme 2 into its specific components. Figure 11 shows the emission from solutions of [$\mathbf{C_8}$] $= 1.2 \times 10^{-7}$ M when in the presence of [$ssDNA_2$-C*] $= 2.0 \times 10^{-8}$ M or [$dsDNA_2$-C*] $= 2.0 \times 10^{-8}$ M. A higher FRET ratio is observed for $ssDNA_2$-C* (10.6) than for $dsDNA_2$-C* (1.4). These data are consistent with a stronger attraction between $\mathbf{C_8}$ and $ssDNA_2$-C*. When [$\mathbf{C_8}$] increases, the FRET ratios for dsDNA-C* and ssDNA-C* become more equal. As shown by Figure 12, by the time that [$\mathbf{C_8}$] $= 2.3 \times 10^{-7}$ M and [$ssDNA_2$-C*] $= 2.0 \times 10^{-8}$ M or [$dsDNA_2$-C*] $= 2.0 \times 10^{-8}$ M, the FRET ratios are nearly the same.

Structural differences between dsDNA and ssDNA account for the concentration effect on FRET. At low concentrations, there is a greater affinity between ssDNA and $\mathbf{C_8}$ as a result of electrostatic interactions and the exposed hydrophobic portion of ssDNA. At higher concentration regimes, a larger number of donor molecules can approach the vicinity of dsDNA because it has a higher number of charges. Consistent with this idea is the fact that after the ratio of $\mathbf{C_8}$ to C* is 6:1 (i.e., approximately a 1:1 charge ratio for ssDNA), the C* emission intensity ceases

(36) Gaylord, B. S.; Heeger, A. J.; Bazan, G. C. *Proc. Natl. Acad. Sci. U.S.A.* **2002**, *99*, 10954.
(37) Pullman, B.; Lavery, R.; Pullman, A. *Eur. J. Biochem.* **1982**, *124*, 229.
(38) Diogo, M. M.; Queiroz, J. A.; Monteiro, G. A.; Martins, S. A. M.; Ferreira, G. N. M.; Prazeres, D. M. F. *Biotechnol. Bioeng.* **2000**, *68*, 576.
(39) Knemeyer, J. P.; Marmé, N.; Sauer, M. *Anal. Chem.* **2000**, *72*, 3717.
(40) Torimura, M.; Kurata, S.; Yamada, K.; Yokomaku, T.; Kamagata, Y.; Kanagawa, T.; Kurane, R. *Anal. Sci.* **2001**, *17*, 155.

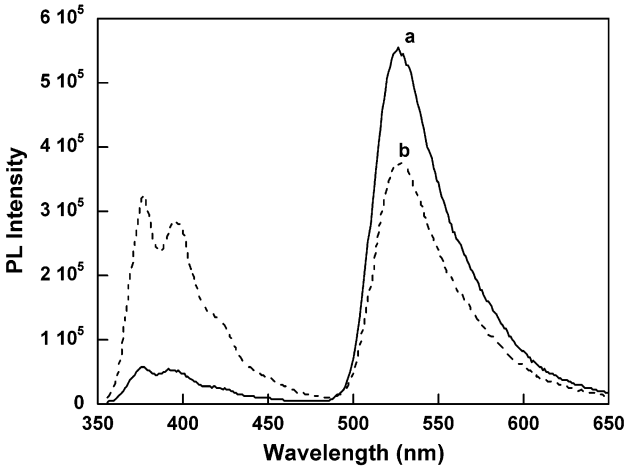

Figure 11. Emission spectra from solutions containing $\mathbf{C_8}$ and ssDNA$_2$-C* (a) and dsDNA$_2$-C* probes (b) in buffer ([ssDNA$_2$-C*] or [dsDNA$_2$-C*] = 2.0×10^{-8} M, [$\mathbf{C_8}$] = 1.2×10^{-7} M). The excitation wavelength was 345 nm for all spectra.

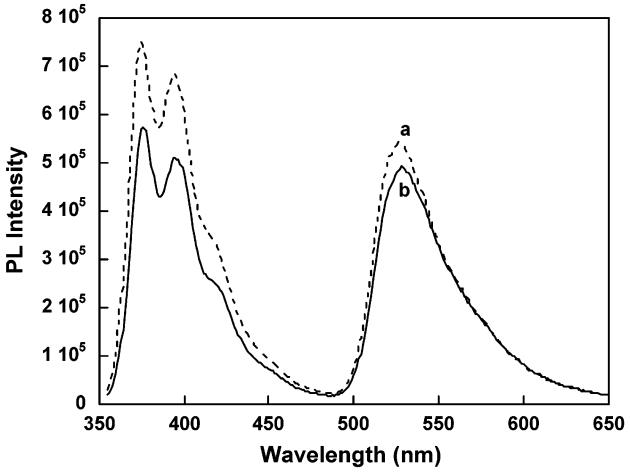

Figure 12. Emission spectra from solutions containing $\mathbf{C_8}$ and (a) ssDNA$_2$-C* and (b) dsDNA$_2$-C* in buffer ([ssDNA$_2$-C*] or [dsDNA$_2$-C*] = 2.0×10^{-8} M, [$\mathbf{C_8}$] = 2.3×10^{-7} M). The excitation wavelength used was 345 nm.

to grow for ssDNA, but continues to increase in the case of dsDNA. Additional charge units remain with the dsDNA structure, which are capable of attracting more $\mathbf{C_8}$ units. However, even after a 12:1 ratio of $\mathbf{C_8}$ to C*, the FRET to ssDNA is slightly higher.

We can now examine how these solutions behave as sensors by comparing the FRET of $\mathbf{C_8}$ to dsDNA$_2$-C* against the FRET to ssDNA$_2$-C* in the presence of a noncomplementary single-stranded DNA (5′-GAC TCA ATG GCG TTA GAC TG). As shown in Figure 13, more efficient energy transfer occurs in the case of dsDNA$_2$-C*. *The lower FRET for the noncomplementary strand thus must arise from a competition between ssDNA-C* and the unhybridized ssDNA, rather than a stronger attraction between $\mathbf{C_8}$ and dsDNA-C*, relative to ssDNA-C**.

Summary and Conclusion

In summary, Scheme 3 provides an improved synthetic entry into cationic water-soluble conjugated oligomers. Suzuki coupling of 2 equiv of the bromide derivatives **4**, **5**, **6**, and **9** with 1,4-phenyldiboronic acid circumvents the difficult chromatographic separation associated with amine-containing fluorene

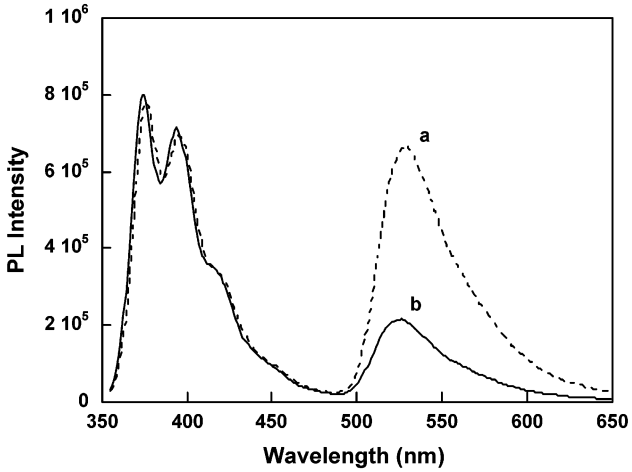

Figure 13. Emission spectra from solutions containing $\mathbf{C_8}$ and (a) a hybridized (dsDNA$_2$-C*) and (b) a nonhybridized (ssDNA$_2$-C* + 5′-GAC TCA ATG GCG TTA GAC TG) ssDNA pair in buffer (([ssDNA$_2$-C*] or [dsDNA$_2$-C*] = 2.0×10^{-8} M, [$\mathbf{C_8}$] = 2.3×10^{-7} M). The spectra are normalized with respect to the $\mathbf{C_8}$ emission.

fragments.[27] Additionally, direct quaternization of the side chains of the fully assembled chromophores simplifies the overall synthetic scheme by one step. The compounds $\mathbf{C_3}$, $\mathbf{C_4}$, $\mathbf{C_6}$, and $\mathbf{C_8}$ provide a series of chromophores that modulates the separation of charged side groups from a common conjugated framework, resulting in varying levels of hydrophobic content.

FRET experiments in water between the tetracationic $\mathbf{C_3}$−$\mathbf{C_8}$ and the pentaanionic chromophore **3** reveal that the most efficient energy transfer occurs with $\mathbf{C_8}$. This result seems at first counterintuitive, if one considers the distance dependence of FRET, together with the longer tether between the chromophore and the charged quaternary nitrogen, and highlights the importance of hydrophobic interactions in this class of compounds. Polar organic compounds, such as methanol, reduce the attraction between the hydrophobic fragments, and one observes a FRET efficiency that increases with shorter thethers; $\mathbf{C_3}$ is most effective.

Similar to **3**, single-stranded DNA provides sites for electrostatic and hydrophobic interactions. In the buffer conditions required for DNA−DNA hybridization, we find that only $\mathbf{C_6}$ and $\mathbf{C_8}$ show efficient FRET to the ssDNA tagged with fluorescein (ssDNA-C*). Increasing electrolyte strength reduces the Coulombic attraction between donor and acceptor molecules, in agreement with standard Debye−Hückel Theory.[34] That in water one observes energy transfer from $\mathbf{C_3}$−$\mathbf{C_8}$ to ssDNA-C* demonstrates that the buffer ions screen electrostatic forces, to the point that they are insufficient for bringing the less hydrophobic chromophores $\mathbf{C_3}$ and $\mathbf{C_4}$ within FRET distance. The effect of salt addition on electrostatic screening in Figures 8 and 9 shows the difference in the binding strength for $\mathbf{C_3}$/ssDNA-C* and $\mathbf{C_8}$/ssDNA-C*. This dependence is in agreement with Bloomfield's calculation to determine the roles of electrostatics and hydrophobicity in the binding of cationic lipids to DNA. From their calculations, every additional methylene group in an aliphatic lipid chain increases the association constant about 4-fold by increasing the binding cooperativity with DNA.[41] It is also noteworthy that double-stranded DNA

(41) Matulis, D.; Rouzina, I.; Bloomfield, V. A. *J. Am. Chem. Soc.* **2002**, *124*, 7331.

Scheme 5. Molecular Structures of **2-C$_3$** and **2-C$_8$**

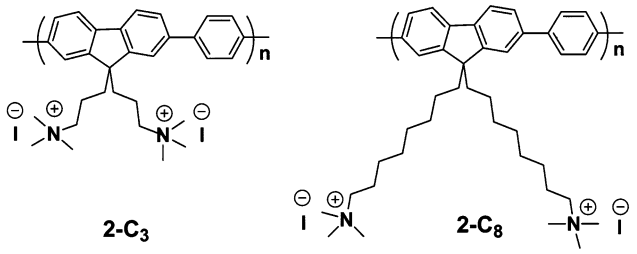

"hides" the hydrophobic component within its helical structure. However, the hydrophobic interactions remain important in determining the FRET efficiency between dsDNA-C* and the donors because only **C$_6$** and **C$_8$** result in measurable FRET when in the presence of buffer.

We have also determined that in these solutions the energy transfer between **C$_8$** and ssDNA is more efficient than that between **C$_8$** and dsDNA (Figure 11), perhaps as a result of ssDNA's more exposed hydrophobic component and more flexible structure. With this information, we have shown that the success of Scheme 2 as a sensor method does not rely on stronger interactions between cationic conjugated polymers and ssDNA or dsDNA. Rather, more efficient FRET occurs with dsDNA-C* because in situation **B** the nonhybridized strands remain in solution and screen the interaction between the conjugated polymer and the tagged ssDNA-C*.

These findings also open up possibilities and guidelines for the design of new biosensor materials. For example, it would seem reasonable that a polymer such as **2-C$_3$** (Scheme 5) would be more sensitive to variations in analyte charge than **2-C$_8$**, for which hydrophobic interactions would be less discriminating. If so, one could generate homogeneous sensory optical reporters that specifically respond to changes in the charge of the target analyte. These studies are underway in our laboratories.

Experimental Section

General Details. ^{1}H and ^{13}C NMR spectra were collected on Varian Inova 400 MHz or Varian ASM-100 200 MHz spectrometers. The UV−vis absorption spectra were recorded on a Shimadzu UV-2401 PC diode array spectrometer. Photoluminescence spectra were obtained on a Spex Fluorolog 2 spectrometer, using 90° angle detection for solution samples. Mass spectrometry and elemental analysis were performed by the UC Santa Barbara Mass Spectrometry Lab and elemental analysis center. Reagents were obtained from Aldrich Co. and used as received.

The oligonucleotide that was used in the single-stranded DNA study (ssDNA$_1$) was the 20 base pair sequence 5′-Fl-CCA ATC AGT CCA GTG ATA CG, containing a fluorescein chromophore at the 5′ position. The oligonucleotides that were used for complementary and noncomplementary studies (ssDNA$_2$) were 5′-Fl-ATC TTG ACT ATG TGG GTG CT and its complementary strand 5′-AGC ACC CAC ATA GTC AAG AT. The noncomplementary strand was the sequence 5′-GAC TCA ATG GCG TTA GAC TG. The samples were prepared by initially determining DNA strand concentrations based on 260 nm absorbance measurements done on 150 μL samples in a 500 μL quartz cuvette using a Shimadzu UV−vis spectrometer. Once the concentration of both strains was established, a 1:1 ratio between complementary single strands was mixed for annealing. The mixtures of complementary strands were annealed at 57.5 °C (2 °C below its melting point of 59.5 °C) for 25 min and then cooled to room temperature slowly, and this was done in an identical fashion for the noncomplementary strands. The absorbance of the hybridized strands was measured to determine their concentration. The extent of hybridization was checked by variable temperature absorbance spectroscopy. Fluorescence intensities were determined from the integrated areas under emission spectra of both the donor and the acceptor fluorescein. The differences in energy transfer were compared by measuring the fluorescence intensity of the acceptor in the presence of the same concentration of the donor.

General Procedure for 2-Bromo-9,9′-bis(ω′′-bromoalkyl)fluorene Compounds. 2-Bromofluorene (1.23 g, 5 mmol) was added to a mixture of aqueous potassium hydroxide (100 mL, 50%), tetrabutylammonium bromide (0.33 g, 1 mmol), and dibromoalkane (50 mmol) at 75 °C. After 15 min, the mixture was cooled to room temperature. After extraction with CH_2Cl_2, the combined organic layers were washed successively with water, aqueous HCl (1 M), water, and brine and then dried over $MgSO_4$. After removal of the solvent and the excess 1,6-dibromoalkane, the residue was purified by silica gel column chromatography using hexane and chloroform (9:1) as the solvent.

2-Bromo-9,9′-bis(3′′-bromopropyl)fluorene (4). Following the procedure described above, we obtained compound **4** as a white solid in a yield of 35%. ^{1}H NMR (200 MHz, $CDCl_3$) δ: 1.09−1.13 (br, 4H), 2.05−2.18 (m, 4H), 3.07−3.14 (t, 4H), 7.35−7.37 (m, 3H), 7.49−7.51 (m, 2H), 7.53−7.58 (m, 1H), 7.60−7.72 (m, 1H). ^{13}C NMR (50 MHz, $CDCl_3$) δ: 27.15, 34.15, 38.74, 54.36, 120.24, 121.52, 122.98, 126.21, 127.85, 128.18, 130.81, 140.18, 140.29, 148.55, 151.23. Anal. Calcd for $C_{19}H_{19}Br_3$: C, 46.85; H, 3.93. Found: C, 47.07; H, 3.99.

2-Bromo-9,9′-bis(6′′-bromohexyl)fluorene (5). Following the procedure described above, we obtained compound **5** as a light yellow oil in a yield of 75%. ^{1}H NMR (200 MHz, $CDCl_3$) δ: 0.60−0.65 (m, 4H), 1.07−1.21 (m, 8H), 1.54−1.71 (m, 4H), 1.91−1.99 (m, 4H), 3.26−3.28 (t, 4H), 7.33−7.36 (m, 3H), 7.45−7.48 (m, 2H), 7.52−7.60 (m, 1H), 7.64−7.72 (m, 1H). ^{13}C NMR (50 MHz, $CDCl_3$) δ: 23.64, 27.94, 29.17, 32.79, 34.13, 40.30, 55.42, 120.03, 121.31, 122.97, 126.21, 127.27, 127.78, 130.23, 140.19, 140.32, 150.08, 152.76. Anal. Calcd for $C_{25}H_{31}Br_3$: C, 52.57; H, 5.47. Found: C, 52.32; H, 5.31.

2-Bromo-9,9′-bis(8′′-bromooctyl)fluorene (6). Following the procedure described above, we obtained compound **6** as a light yellow oil in 80% yield. ^{1}H NMR (200 MHz, $CDCl_3$) δ: 0.50−0.62 (m, 4H), 1.01−1.07 (m, 12H), 1.21−1.35 (br, 4H), 1.68−1.80 (m, 4H), 1.90−1.98 (m, 4H), 3.30−3.32 (t, 4H), 7.32−7.34 (br, 3H), 7.42−7.46 (m, 2H), 7.52−7.58 (m, 1H), 7.62−7.70 (m, 1H). ^{13}C NMR (50 MHz, $CDCl_3$) δ: 23.76, 28.20, 28.73, 29.13, 29.92, 32.90, 34.23, 40.39, 55.49, 119.97, 121.25, 123.00, 126.25, 127.16, 127.70, 130.11, 140.15, 140.30, 150.29, 152.99. Anal. Calcd for $C_{29}H_{39}Br_3$: C, 55.52; H, 6.27. Found: C, 55.78; H, 6.51.

4-Bromo-1-(4′-methylphenyloxy)butane (7). A mixture of 1,4-dibromobutane (50 mL), potassium carbonate (27.6 g, 200 mmol), 4-methylphenol (6.49 g, 60 mmol), and a catalytic amount of 18-crown-6 in 400 mL of acetone was refluxed for 2 days. After removal of the acetone, the residue was poured into water and was extracted with diethyl ether (3 × 100 mL). The combined organic layer was washed with aqueous HCl (1 M) and then with water. After being dried and removal of the solvent, the residue was distilled under vacuum to afford **7** (10.5 g, 75%) as a colorless oil. ^{1}H NMR (200 MHz, $CDCl_3$) δ: 1.88−2.11 (m, 4H), 2.29 (s, 3H), 3.46−3.53 (t, 2H), 3.94−4.0 (t, 2H), 6.77−6.81 (d, 2H), 7.06−7.11 (d, 2H). ^{13}C NMR (50 MHz, $CDCl_3$) δ: 20.74, 30.40, 32.68, 65.52, 69.02, 114.61, 130.16, 130.30, 156.80.

2-Bromo-9,9′-bis(4′′-methylphenyloxybutyl)fluorene (8). Following the same procedure as described for the 2-bromo-9,9′-bis(ω′′-bromoalkyl)fluorene compounds, after silica gel chromatography using hexane and chloroform (3:1) as the eluent, we obtained compound **8** as white crystals (65%). ^{1}H NMR (200 MHz, $CDCl_3$) δ: 0.72−0.83 (m, 4H), 1.46−1.57 (m, 4H), 1.98−2.06 (m, 4H), 2.25 (s, 6H), 3.65−3.72 (t, 4H), 6.63−6.69 (d, 4H), 6.99−7.04 (d, 4H), 7.31−7.34 (m, 3H), 7.43−7.48 (m, 2H), 7.49−7.53 (m, 1H), 7.58−7.68 (m, 1H). ^{13}C NMR (50 MHz, $CDCl_3$) δ: 20.46, 20.61, 29.60, 40.12, 55.41, 67.67, 114.47, 120.07, 121.35, 123.03, 126.25, 127.35, 127.83, 129.80, 129.94, 130.33, 140.18, 140.32, 149.78, 152.44, 156.89. Anal. Calcd for $C_{35}H_{37}BrO_2$: C, 73.81; H, 6.55. Found: C, 73.89; H, 6.83.

2-Bromo-9,9′-bis(4″-bromobutyl)fluorene (9). A mixture of 2-bromo-9,9-bis(4-methylphenyloxybutyl)fluorene (91.0 g, 17.5 mmol), 4 mL of 48% HBr, and 20 mL of acetic acid was refluxed for 2 days. The reaction mixture was poured into water, and the resulting solution was extracted with chloroform (3 × 50 mL). The combined organic layers were washed with dilute aqueous Na_2CO_3 (1 M, 2 × 50 mL) and water and were dried over $MgSO_4$. The solvent was removed, and the resulting oil was purified by silica gel chromatography using hexane and chloroform (7:1) as the eluent to afford **9** (580 mg, 64%) as a colorless oil, which solidified upon standing. ^{1}H NMR (200 MHz, $CDCl_3$) δ: 0.69−0.81 (m, 4H), 1.55−1.69 (m, 4H), 1.97−2.02 (m, 4H), 3.12−3.19 (t, 4H), 7.32−7.38 (m, 3H), 7.45−7.54 (m, 2H), 7.56−7.59 (m, 1H), 7.68−7.70 (m, 1H). ^{13}C NMR (50 MHz, $CDCl_3$): 22.69, 33.21, 33.33, 39.41, 55.13, 120.25, 121.53, 123.00, 126.26, 127.61, 128.01, 130.56, 140.18, 140.30, 149.37, 152.07. Anal. Calcd for $C_{21}H_{23}Br_3$: C, 48.96; H, 4.50. Found: C, 48.83; H, 4.64.

General Procedure for 1,4-Bis(9,9′-bis(ω″-bromoalkyl)-2′fluorenyl)benzene. A mixture of 2-bromo-9,9′-bis(ω″-bromoalkyl)fluorene (1.05 mmol), 1,4-phenyldiboronic acid (0.5 mmol), $Pd(PPh_3)_4$ (10 mg), and sodium carbonate (5 mmol) in 10 mL of THF and 2.5 mL of water was degassed and stirred at 80 °C for 48 h. The mixture was cooled to room temperature and diluted with 100 mL of chloroform. The organic layer was collected, washed with water and then brine, dried over magnesium sulfate, and then the solvent was removed. The residue was adsorbed on silica gel and purified by chromatography (hexane: toluene = 1:1 to 1:3) to give the desired compounds in yields from 35% to 60%.

1,4-Bis(9,9′-bis(3″-bromopropyl)-2′-fluorenyl)benzene (10). Precursor oligomer **10** was obtained as a white powder in a yield of 35%. ^{1}H NMR (200 MHz, $CDCl_3$) δ: 1.20−1.25 (m, 8H), 2.22−2.27 (m, 8H), 3.10−3.17 (t, 8H), 7.37−7.39 (m, 6H), 7.65−7.78 (m, 12H). ^{13}C NMR (50 MHz, $CDCl_3$) δ: 27.30, 34.56, 38.88, 54.23, 120.25, 120.49, 121.48, 122.98, 126.71, 127.78, 140.23, 140.49, 140.55, 140.83, 149.24, 149.78. MS (MALDI-TOF): 890.2 (M), 810.2 (M − Br), 730.2 (M − 2Br), 650.2 (M − 3Br). Anal. Calcd for $C_{44}H_{42}Br_4$: C, 59.35; H, 4.75. Found: C, 59.17; H, 4.75.

1,4-Bis(9,9′-bis(4″-bromobutyl)-2′-fluorenyl)benzene (11). Precursor oligomer **11** was obtained as a white powder in a yield of 44%. ^{1}H NMR (200 MHz, $CDCl_3$) δ: 0.79−0.86 (br, 8H), 1.58−1.69 (m, 8H), 2.03−2.10 (m, 8H), 3.16−3.22 (t, 8H), 7.35−7.39 (br, 6H), 7.63−7.83 (m, 12H). ^{13}C NMR (50 MHz, $CDCl_3$) δ: 22.72, 33.23, 33.36, 39.54, 54.89, 120.17, 120.40, 121.43, 122.93, 126.43, 127.45, 127.53, 127.76, 139.98, 140.50, 140.63, 140.87, 150.03, 150.49. MS (MALDI-TOF): 946 (M), 866 (M − Br), 786 (M − 2Br). Anal. Calcd for $C_{48}H_{50}Br_4$: C, 60.91; H, 5.32. Found: C, 61.05; H, 5.32.

1,4-Bis(9,9′-bis(6″-bromohexyl)-2′-fluorenyl)benzene (12). Precursor oligomer **12** was obtained as a white powder in a yield of 55%. ^{1}H NMR (200 MHz, $CDCl_3$) δ: 0.67−0.71 (m, 8H), 1.10−1.26 (m, 16H), 1.60−1.71 (m, 8H), 2.00−2.08 (m, 8H), 3.29 (t, 8H), 7.35−7.39 (m, 6H), 7.61−7.68 (m, 4H), 7.73−7.82 (m, 8H). ^{13}C NMR (50 MHz, $CDCl_3$) δ: 23.75, 27.92, 29.24, 32.80, 34.19, 40.43, 55.20, 120.03, 120.26, 121.44, 122.97, 126.14, 127.15, 127.37, 127.74, 139.76, 140.57, 140.69, 140.89, 150.76, 151.24. MS (MALDI-TOF): 1058 (M), 978 (M − Br), 898 (M − 2Br), 818 (M − 3Br). Anal. Calcd for $C_{56}H_{66}Br_4$: C, 63.53; H, 6.28. Found: C, 64.33; H, 6.45.

1,4-Bis(9,9′-bis(8″-bromooctyl)-2′-fluorenyl)benzene (13). Precursor oligomer **13** was obtained as a colorless oil in a yield of 60%. ^{1}H NMR (200 MHz, $CDCl_3$) δ: 0.69 (br, 8H), 1.07 (br, 24H), 1.25−1.32 (m, 8H), 1.61−1.81 (m, 8H), 1.98−2.06 (m, 8H), 3.29−3.36 (m, 8H), 7.33−7.38 (m, 6H), 7.60−7.81 (m, 12H). ^{13}C NMR (50 MHz, $CDCl_3$) δ: 24.09, 28.44, 29.00, 29.38, 30.24, 33.15, 34.52, 37.36, 40.79, 55.53, 118.33, 120.23, 120.45, 121.76, 123.27, 126.27, 127.29, 127.53, 127.96, 129.46, 140.00 140.34, 140.64, 141.16, 151.27, 151.75. MS (MALDI-TOF): 1170.6 (M), 1090.6 (M − Br), 1010.7 (M − 2Br), 930.7 (M − 3Br). Anal. Calcd for $C_{64}H_{82}Br_4$: C, 65.65; H, 7.06. Found: C, 65.06; H, 6.45.

General Procedure for 1,4-Bis(9,9′-bis(ω″-(*N*,*N*,*N*-trimethylammonium)-alkyl)-2′-fluorenyl)benzene Tetrabromide (C_3, C_4, C_6, and C_8). The precursor oligomer (100 mg) was dissolved in 10 mL of THF and was then diluted with 5 mL of water. After the mixture was cooled to − 78 °C, condensed trimethylamine (1 mL) was added dropwise. The mixture was stirred at − 78 °C for 12 h and was then gradually warmed to room temperature. After an additional 24 h, the THF and water were removed, and the residue was recrystallized from ethanol to yield the target oligomers with yields of 40−75%.

1,4-Bis(9,9′-bis(3″-(*N*,*N*,*N*-trimethylammonium)-propyl)-2′-fluorenyl)benzene Tetrabromide (C_3). Oligomer $\mathbf{C_3}$ was obtained as a white powder in a yield of 40%. ^{1}H NMR (500 MHz, D_2O, 90 °C) δ: 1.64−1.70 (m, 8H), 2.82−2.89 (m, 8H), 3.30−3.34 (s, 36H), 3.52−3.55 (m, 8H), 8.10−8.58 (m, 18H). ^{13}C NMR (125 MHz, D_2O, 90 °C) δ: 18.76, 36.38, 53.77, 55.53, 67.69, 121.53, 121.96, 122.68, 124.83, 128.02, 128.66, 129.38, 129.5, 140.75, 140.84, 141.73, 141.82, 149.74, 150.56. MS (ESI-MS): 1047 $(M - Br)^+$, 483 $(M - 2Br)^{2+}$, 295 $(M - 3Br)^{3+}$, 201 $(M - 4Br)^{4+}$.

1,4-Bis(9,9′-bis(4″-(*N*,*N*,*N*-trimethylammonium)-butyl)-2′-fluorenyl)benzene Tetrabromide (C_4). Oligomer $\mathbf{C_4}$ was obtained as a white powder in a yield of 65%. ^{1}H NMR (500 MHz, D_2O, 90 °C) δ: 1.20−1.41 (m, 8H), 1.90−1.92 (br, 8H), 2.68−2.72 (m, 8H), 3.36−3.48 (m, 44H), 7.74−8.58 (m, 18H). ^{13}C NMR (125 MHz, D_2O, 90 °C) δ: 21.98, 23.51, 39.08, 54.03, 56.11, 67.51, 121.16, 121.75, 122.22, 125.06, 126.82, 128.36, 128.79, 129.10, 139.28, 140.06, 141.17, 141.69, 151.57, 152.42. MS (ESI-MS): 1104 $(M - Br)^+$, 511 $(M - 2Br)^{2+}$, 315 $(M - 3Br)^{3+}$, 216 $(M - 4Br)^{4+}$.

1,4-Bis(9,9′-bis(6″-(*N*,*N*,*N*-trimethylammonium)-hexyl)-2′-fluorenyl)benzene Tetrabromide (C_6). Oligomer $\mathbf{C_6}$ was obtained as a white powder in a yield of 75%. ^{1}H NMR (500 MHz, D_2O, 90 °C) δ: 1.02 (m, 8H), 1.33−1.35 (br, 16H), 1.76−1.79 (m, 8H), 2.20−2.30 (m, 4H), 2.45 (m, 4H), 3.39−3.50 (m, 44H), 7.95−8.12 (m, 12 H), 8.39−8.54 (m, 6H). ^{13}C NMR (125 MHz, D_2O, 90 °C) δ: 23.10, 24.54, 26.13, 29.33, 31.32, 39.88, 54.08, 56.23, 67.64, 120.85, 121.58, 121.69, 124.94, 126.59, 128.24, 128.37, 128.82, 138.99, 140.34, 141.28, 141.60, 152.41, 153.09. MS (ESI-MS): 566 $(M - 2Br)^{2+}$, 351 $(M - 3Br)^{3+}$, 293 $(M - 4Br)^{4+}$.

1,4-Bis(9,9′-bis(8″-(*N*,*N*,*N*-trimethylammonium)-octyl)-2′-fluorenyl)benzene Tetrabromide (C_8). Oligomer $\mathbf{C_8}$ was obtained as a white powder in a yield of 72%. ^{1}H NMR (500 MHz, D_2O, 90 °C) δ: 1.03−1.05 (br, 8H), 1.20−1.26 (br, 16 H), 1.26−1.30 (br, 16H), 1.45−1.48 (br, 8H), 1.88−1.90 (br, 4H), 2.36 (br, 4H), 3.52−3.60 (br, 44H), 7.90−8.00 (m, 6H), 8.24−8.28 (br, 8H), 8.71 (br, 4H). ^{13}C NMR (125 MHz, D_2O, 90 °C) δ: 23.48, 25.15, 26.79, 29.40, 29.54, 29.87, 30.50, 40.69, 54.22, 56.11, 67.81, 120.86, 121.65, 124.70, 126.82, 128.36, 128.45, 128.57, 139.63, 141.07, 141.52, 141.63, 152.30, 152.97. MS (ESI-MS): 1327 $(M - Br)^+$, 624 $(M - 2Br)^{2+}$, 389 $(M - 3Br)^{3+}$, 272 $(M - 4Br)^{4+}$.

Acknowledgment. The authors are grateful to the ONR (N00014-98-1-0759), the NSF (DMR-0097611), and the NIH (GM62958-01) for financial support and to Professors Alan Heeger and Kevin Plaxco for useful discussions.

JA028961W